


**COVER PAGE**

***Document downloaded by @DAEL***

***Wed Nov 25 16:42:33 2026***
***For personal use***

When automatic English translation is provided, only the original document is authentic.
The EAA cannot be held responsible of any translation error

Bibliographical reference

*Spindle-Torus Sampling for an Efficient-Scanning Spherical Microphone Array*, David L. Alon and Boaz Rafaely, Acta Acustica **vol. 98** (Number 1), 2012, pp. 83-90

DOI
https://doi.org/10.3813/AAA.918494

**Acta Acustica united with Acustica**
**Vol. 98 (2012) 83 – 90**

DOI 10.3813/AAA.918494

# Spindle-Torus Sampling for an Efficient-Scanning Spherical Microphone Array

David L. Alon, Boaz Rafaely
Department of Electrical and Computer Engineering, Ben-Gurion University of the Negev, Beer-Sheva 84105, Israel. davidalo@bgu.ac.il, br@ee.bgu.ac.il

**Summary**
Spherical microphone arrays have been studied for a wide range of applications. In particular, microphones arranged around an open sphere in scanning microphone array configurations are useful for sound field analysis. However, it has been shown that open-sphere arrays have poor robustness at the null frequencies of the spherical Bessel functions. Alternative configurations that overcome this problem have been presented, including the dual-sphere configuration, which requires to double the total number of spatial samples, and the shell configuration, which is difficult to implement with a scanning system. This paper presents a new spindle-torus sampling configuration, which achieves high robustness with a relatively small number of sampling points. The special geometry of the torus surface is realized using two rotating tables and a mechanical offset, which facilitates conducting a measurement session with a fully automatic scanning using a single microphone.

**PACS no. 43.60.Fg**

## 1. Introduction

Spherical microphone arrays are widely studied and used for sound field measurement and analysis. The spherical array configuration is advantageous due to its symmetry, which simplifies spatial sound field analysis in three dimensions and allows efficient spherical harmonics domain processing [1, 2, 3]. One way to construct a spherical microphone array is to mount microphones on the surface of a rigid sphere [1]. Rigid-sphere microphone arrays are limited by size and number of microphones due to practical constraints such as cost, mobility and the undesired scattering effect of the array on the measured sound field. Limitations on array size make this method less practical, particularly at low frequencies, where large arrays are required. Furthermore, limiting the number of microphones limits the achievable spatial resolution of the array [3]. Another method to construct a spherical array is around an open sphere. In this method microphones are typically placed on the surface of a virtual sphere in a free field. Open-sphere arrays can be implemented using a single microphone or a few microphones making measurements in a sequence. This configuration is referred to as a scanning microphone array configuration and is suitable only in applications that do not require real-time or simultaneous recording by all microphones. A scanning array based on a single-sphere configuration is simple to implement mechanically, as it only requires a single pressure microphone fixed on a boom and two rotating tables controlling the elevation and the azimuth of the boom. This simple implementation allows flexibility in array design. First, the frequency range of operation is determined by changing the length of the rotating boom. Second, the spatial resolution of the array is controlled by selecting a sampling scheme with an appropriate number of sampling points. In applications such as room acoustics measurement and analysis, this flexibility is an advantage and the scanning array can therefore be considered more suitable than the rigid-sphere array. On the other hand, it has been shown that, unlike the rigid-sphere, open-sphere configurations suffer from numerical ill-conditioning at frequencies related to the zeros of the spherical Bessel functions [4]. For these reasons, alternative open-sphere configurations have been proposed, such as the dual-sphere configuration [4] and the spherical-shell configuration [5]. However, these configurations have drawbacks. The dual-sphere configuration requires twice as many samples compared to the single-sphere configuration, either using two microphones at two different radii, or changing the radius of the microphone half-way into the scanning measurement session. The spherical-shell configuration is efficient in terms of the total number of samples, which is the same as for the single-sphere array. It requires to position microphones inside the volume of a shell, which cannot be realized by a simple two-motor scanning system.

The method proposed in this paper combines the advantages of the two previously proposed methods, namely the dual-sphere and the spherical-shell arrays, while at the same time avoiding their shortcomings. First, similar to the dual-sphere configuration [4], the implementation of the mechanical system based on a single pressure scanning microphone attached to a rotating boom is relatively simple. Second, the samples in this configuration cover a

Received 3 March 2011,
accepted 18 September 2011.

© S. Hirzel Verlag · EAA


*Document downloaded by @DAEL, 2026-11-25 16:42:36 - personal use only*

volume defined by a spindle-torus surface [6], similar to the volume in the spherical-shell configuration, so high array robustness is achieved without increasing the number of sampling points [7]. Furthermore, due to the special mechanical offset between the two rotating tables, no adjustment of the boom length is required within a measurement session and it is sufficient to use a single microphone. To summarize, the proposed method requires the same number of samples and allows a simple realization with a single microphone and a two-motors scanning system, as in the single-sphere configuration. Concurrently, it offers high robustness at the spherical Bessel nulls as in the dual-sphere and spherical-shell configuration.

This paper is organized as follows. Section 2 reviews the theory of spherical microphone array processing. The following section gives an overview on different array configurations that can be found in the literature. Section 4 details the proposed spindle-torus configuration, and section 5 discusses the distribution of sampling points on the spindle-torus surface. A detailed study of simulation and measurement data is given in sections 6 and 7, respectively.

## 2. Spherical microphone array processing

Consider a sound field with the pressure denoted by $p(k, r, \theta, \phi)$, where $k$ is the wave number, $r$ is the distance from the spatial location to the origin, $\theta$ is the zenith angle from the $z-axis$ and $\phi$ is the azimuthal angle along the $xy-plane$ from the $x-axis$ counterclockwise. Microphone array processing based on spherical harmonics has been recently presented [1, 8]. In this section, we provide a brief review of this theory. The goal here is to find the plane waves composing the sound field, given the sound pressure measured by the spherical array.

We start by describing the pressure on a virtual open sphere. The pressure is due to a unit amplitude incident plane wave, arriving from $(\theta_l, \phi_l)$, with wave number $k$ and measured at position $(r, \theta, \phi)$. Using spherical harmonics, the pressure can be written as [9]

$$p_l(k, r, \theta, \phi) = \sum_{n=0}^{\infty} \sum_{m=-n}^{n} b_n(kr)\, Y_n^{m^*}(\theta_l, \phi_l)\, Y_n^m(\theta, \phi), \quad (1)$$

where $b_n(kr)$ is generalized for various array configurations [4] and particularly for single open-sphere pressure microphone arrays $b_n(kr) = 4\pi i^n j_n(kr)$, where $i = \sqrt{-1}$ and $j_n$ denotes the spherical Bessel function of order $n$. $Y_n^m(\theta, \phi)$ represent the spherical harmonics of order $n$ and degree $m$. Taking the spherical Fourier transform of $p_l(k, r, \theta, \phi)$, and using the orthogonality property of spherical harmonics, we get

$$p_{l_{nm}}(k, r) = b_n(kr)\, Y_n^{m^*}(\theta_l, \phi_l). \quad (2)$$

For the more general case, where the sound field is composed of an infinite number of plane waves having spatial amplitude density $a(k, \theta, \phi)$, $p_{nm}$ can be written as [3]

$$p_{nm}(k, r) = a_{nm}(k)\, b_n(kr), \quad (3)$$

where $a_{nm}(k)$ is spherical Fourier transform of $a(k, \theta, \phi)$.

Plane wave decomposition can now be performed by dividing the spherical Fourier coefficients of the pressure, $p_{nm}$, by $b_n$. When the magnitude of $b_n$ is small, the division may become numerically ill-conditioned. This may be the case when the microphone positions are restricted to a single sphere, see section 3. Equation (3) can be rewritten in matrix form by taking the inverse spherical Fourier transform of $p_{nm}$. This facilitates the representation of the sound pressure at positions, which are not restricted to a single sphere,

$$\mathbf{p} = \mathbf{B}\mathbf{a}_{nm} \quad (4)$$

where $\mathbf{a}_{nm} = \left[ a_{00}(k) \;\; a_{1(-1)}(k) \;\cdots\; a_{NN}(k) \right]^T$ and $\mathbf{p} = \left[ p(k, r_1, \theta_1, \phi_1) \;\cdots\; p(k, r_M, \theta_M, \phi_M) \right]^T$ are column vectors of length $(N+1)^2$ and $M$, respectively.

We assume that the pressure can be accurately described by a limited spherical harmonics order $N$, typically for frequencies that satisfy $kr \leq N$ [8, 4], and is sampled at $M$ positions, $(r_m, \theta_m, \phi_m)$, $1 \leq m \leq M$. As shown by Rafaely [5], in this case we can compute the spherical Fourier transform of the plane wave amplitude density $\mathbf{a}_{nm}$ by

$$\mathbf{a}_{nm} = \mathbf{C}\mathbf{p}. \quad (5)$$

Matrix $\mathbf{C}$ can be calculated using matrix $\mathbf{B}$ of size $M \times (N+1)^2$ defined as

$$\mathbf{B} = \begin{bmatrix} b_0(kr_1)\, Y_0^0(\Omega_1) & \cdots & b_0(kr_M)\, Y_0^0(\Omega_M) \\ b_1(kr_1)\, Y_1^{-1}(\Omega_1) & \cdots & b_1(kr_M)\, Y_1^{-1}(\Omega_M) \\ b_1(kr_1)\, Y_1^0(\Omega_1) & \cdots & b_1(kr_M)\, Y_1^0(\Omega_M) \\ b_1(kr_1)\, Y_1^1(\Omega_1) & \cdots & b_1(kr_M)\, Y_1^1(\Omega_M) \\ \vdots & \ddots & \vdots \\ b_N(kr_1)\, Y_N^N(\Omega_1) & \cdots & b_N(kr_M)\, Y_N^N(\Omega_M) \end{bmatrix}^T, \quad (6)$$

where $(\Omega_M) = (\theta_M, \phi_M)$, and $\mathbf{C}$ is given by

$$\mathbf{C} = \mathbf{B}^{\dagger}. \quad (7)$$

Matrix $\mathbf{B}^{\dagger}$ is the pseudo inverse of matrix $\mathbf{B}$, $\mathbf{B}^{\dagger} = \left(\mathbf{B}^H\mathbf{B}\right)^{-1}\mathbf{B}^H$, assuming $M > (N+1)^2$ . Furthermore, an error in the solution originating from model errors or measurement noise may be multiplied by the condition number of matrix $\mathbf{B}$. We therefore wish to design a microphone array with a minimal condition number of matrix $\mathbf{B}$, facilitating greater array robustness.

## 3. Previously investigated configurations

### 3.1. Scanning microphone arrays

In an open-sphere array configuration, microphones are typically placed on the surface of a virtual sphere in free field. One way to implement open-sphere arrays is by making sequential measurements with a single or a few microphones, in a configuration referred to as a scanning microphone array configuration. This configuration is suitable in applications that do not require simultaneous recordings



*Document downloaded by @DAEL, 2026-11-25 16:42:36 - personal use only*

of all microphone signals. The microphones are typically mounted on a boom and rotated in space using a mechanical apparatus and a set of motors. Different positions of the microphone represent different spatial samples of the microphone array. Unlike a real-time array configuration, the number of spatial samples in this case is not limited so that a much larger spatial resolution can be achieved, compared to real-time array systems, thereby enabling accurate capture of complex sound fields. The length of the boom holding the microphone determines the radius of the open sphere and so analysis of lower frequencies can be performed simply by extending the length of the boom. Scanning microphone array systems are suitable for offline processing applications, such as sound field analysis in auditorium and room acoustics.

### 3.2. Single open-sphere array

A single open-sphere array configuration is simple to implement when using a scanning microphone array system, as described above. This configuration suffers from ill-conditioning at frequencies related to the zeros of the spherical Bessel functions. The ill-conditioning makes this configuration less appropriate for the standard plane wave decomposition analysis [4].

### 3.3. Dual open-sphere array

A dual-sphere configuration achieves high robustness by combining data from measurements made over two radii and thus is a practical approach for a robust array configuration [4]. However, this advantage comes at the expense of using twice as many microphones (or spatial sampling points) compared to the single-sphere configuration. In this configuration, the information from microphone samples from only one of the spheres is used in the calculation for each frequency. Another shortcoming of the dual-sphere configuration is that an adjustment of the second radius has to be made within the measurement session or, alternatively, two microphones rather than one have to be employed in the measurement process. A method for finding the optimal ratio of the two radii was also presented and will be used in this paper [4].

### 3.4. Spherical-shell array

The spherical shell is another configuration where each microphone is placed at a different radius and direction in the volume enclosed by two concentric spheres. The advantage of this method is that it achieves high robustness without increasing the number of microphones, compared to the single-sphere configuration. In the paper by Rafaely [5], a comparison of different array configurations is performed by computing the condition number of matrix **B** related to each configuration. Array configurations with lower condition numbers are considered more robust to noise and system uncertainties and are therefore preferable in this respect. The shortcoming of the spherical-shell configuration is that the irregular distribution of microphones in space makes it less suitable for a scanning microphone array system.

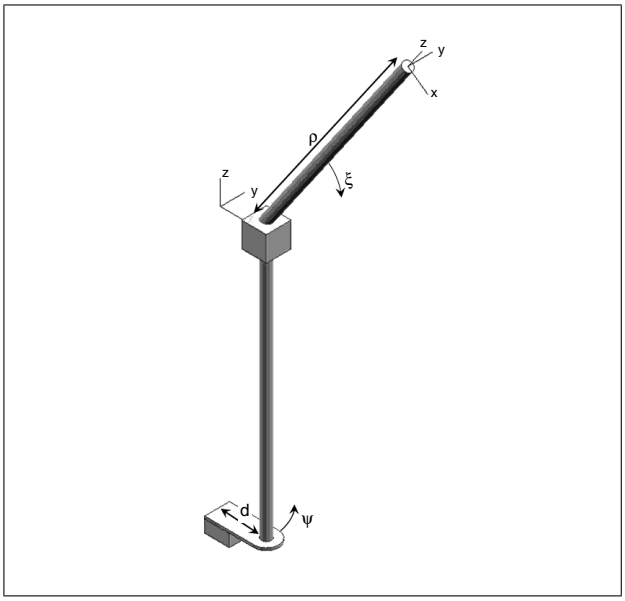



Figure 1. Spindle-torus scanning microphone array mechanical system.

In the next section we present the spindle-torus microphone array, which combines the advantages of the three configurations discussed in this section.

## 4. Spindle-torus microphone array

This section presents a new scanning microphone array configuration, based on a single pressure microphone attached to a boom that is mounted on a vertical rod using two rotating tables. The mechanical configuration is similar to that of a single-sphere scanning microphone array, which is relatively simple to implement. However, in the proposed configuration a mechanical offset between the two rotating tables generates an off-axis system. This mechanical system allows a constrained motion of the microphone in $\mathbb{R}^3$. By rotating the tables, a spindle-torus [6] surface is generated by the microphone positions. As opposed to the dual-sphere configuration, where an adjustment of the second radius has to be made within the measurement session, this geometry allows a fully automatic measurement session with a single scanning microphone and only two rotating tables. Furthermore, similar to the spherical-shell configuration, each microphone is located at a different radius and so high robustness can be achieved without increasing the number of microphones, in comparison with a single-sphere configuration. A schematic illustration of the mechanical system and an illustration of the spindle-torus surface geometry are presented in Figures 1 and 2, respectively.

### 4.1. Spindle-torus surface geometry

In this section we will formulate the geometry of the spindle-torus surface using a linear transformation. To de-



Document downloaded by @DAEL, 2026-11-25 16:42:36 - personal use only

scribe the proposed mechanical system we first define the center of the volume enclosed by the spindle torus as the origin of the global coordinate system. Let $d$ be the mechanical offset between the two rotating tables, and $\rho$ the length of the rotating boom attached to the microphone. The first rotating table performs a rotation in the azimuth direction denoted by $\psi$. This rotation is followed by a translation $d$ of the second rotating table away from the azimuth rotation axis. The rotating boom is mounted on the second rotating table, which controls the elevation $\xi$. The angles $\xi$ and $\psi$ act in the same way as $\theta$ and $\phi$, respectively, in the standard spherical coordinate system [10]. However, unlike the ordinary elevation angle $\theta \in [0, \pi]$, $\xi$ is limited to a larger range, $\xi \in [0, 2\pi)$, which allows the generation of two surfaces that create the spindle-torus shape, rather than a single sphere (see Figure 2). The equation in Cartesian coordinates describing the spindle torus is given by the general equation for a torus with an azimuthal symmetry about the z-axis [6]

$$\left(d - \sqrt{x^2 + y^2}\right)^2 + z^2 = \rho^2. \tag{8}$$

The position of the microphone is determined by the parametric equation

$$\begin{pmatrix} x \\ y \\ z \end{pmatrix} = \begin{pmatrix} d\cos(\psi) + \rho\cos(\psi)\sin(\xi) \\ d\sin(\psi) + \rho\sin(\psi)\sin(\xi) \\ \rho\cos(\xi) \end{pmatrix}, \tag{9}$$

which can be described by two linear transformations. First, an azimuthal rotation by an angle of $\psi$ and a mechanical offset $d$ and second, an elevation of the rotating boom of length $\rho$ by an angle of $\xi$.

The parametric equation implies that the mechanically constrained spindle torus has a total of four degrees of freedom. Each one of the four parameters, $d, \rho, \psi$ or $\xi$, controls the position of the microphone. Given $\psi \in [0, 2\pi)$ and $\xi \in [0, 2\pi)$, the shape of the spindle-torus surface is completely determined by the ratio of the two mechanical parameters $d$ and $\rho$. For a small ratio $d/\rho$, the two surfaces merge and for $d = 0$ we get two concentric spheres with equal radii. When $d/\rho$ is larger than unity, a standard round torus (doughnut shape) [6] rather than a spindle torus is generated. For a constant ratio $d/\rho$, extending the length of the rotating boom $\rho$, will generate a larger array, which will be more desirable for low frequencies.

Representing a rotation followed by a translation with a single linear transformation matrix may be facilitated by the use of homogeneous coordinates [11]. Using a homogeneous transformation matrix, a translation can be expressed as a matrix multiplication. This can be achieved by increasing the dimension of the transformation matrix by one to include the translation part. Such a representation is widely used in projective geometry, and may be used for the investigation of mechanical configurations with more degrees of freedom.

### 4.2. Mechanical offset setting

This study of the spindle-torus configuration is motivated by the work of Balmages and Rafaely [4], in which a dual open-sphere configuration was proposed to avoid zeros of $j_n(kr)$. An optimal ratio of the two radii was derived, such that a zero of $j_n(kr)$ for one of the radii means that for the other radius, $j_n(kr)$ will not be close to zero at the same values of $k$ and $n$. This reflects directly on the behavior of matrix $\mathbf{B}$. In the case of a single open-sphere array, in which all microphones are positioned at the same radius, the existence of a zero, such that $j_n(kr) = 0$ for a given value of $k$ and $n$, will impose one or more columns of zeros in matrix $\mathbf{B}$. These, in turn, will lead to a lower rank of matrix $\mathbf{B}$ and to numerical errors when attempting to compute the matrix inverse. Furthermore, even at frequencies close to the zero frequency, matrix $\mathbf{B}$, although of full rank, may be ill-conditioned, leading to numerical instabilities and poor array robustness against noise and other measurement uncertainties. In the dual-sphere configuration, due to the dual radii, the existence of a column of zeros in matrix $\mathbf{B}$ due to one radius, means that there is another non-zero column due to the second radius, and so rank reduction is avoided.

In the spindle-torus configuration, microphones are distributed over two virtual surfaces, as illustrated in Figure 2. The distance from each microphone position to the origin is referred to as radius $r$. Microphone positions with different elevation angles have different radii. Radii of sampling points over the external surface are in the range $\sqrt{\rho^2 - d^2} \leq r_{ext} \leq d + \rho$, and the radii of sampling points over the internal surface are in the range $\rho - d \leq r_{int} < \sqrt{\rho^2 - d^2}$. Let $\alpha_{st}$ be the ratio between the mean radius of external and internal surfaces $\alpha_{st} = \bar{r}_{ext}/\bar{r}_{int}$, where $\bar{r}_{ext}, \bar{r}_{int}$ are the mean values of the external and internal spindle-torus surfaces radii, respectively. We wish to find the optimal ratio $\alpha_{opt}$ that provides the lowest condition number of matrix $\mathbf{B}$ and highest robustness of the microphone array. Since a rigid-sphere array configuration does not suffer from ill-conditioning due to the zeros of the spherical Bessel functions, its condition number can be considered as a reference for the condition number of open-sphere arrays. We define a criterion $J(\alpha_{st})$ to examine values of $\alpha_{st}$ for maximizing the robustness of the array. The optimal value can be calculated as

$$\alpha_{opt} = \arg\max_{\alpha_{st}} J(\alpha_{st}) \tag{10}$$

and the cost function is defined as

$$J(\alpha_{st}) = \min_k \left\{ \frac{\mathrm{cond}\left(\mathbf{B}_{\mathbf{rigid}}(\mathbf{k})\right)}{\mathrm{cond}\left(\mathbf{B}_{\mathbf{st}}(\mathbf{k})\right)} \right\}. \tag{11}$$

The minimization over $k$ is taken in the array operating frequency range, which is usually defined by array parameters such as the array order $N$, and $\bar{r}_{st}$. Note that the value of $\bar{r}_{st}$ depends on the values of the parameters $\rho$ and $d$. The array order is defined by the number of sampling points $M$, and the selected sampling scheme. Several types of sampling schemes are presented in the next section.



Document downloaded by @DAEL, 2026-11-25 16:42:36 - personal use only

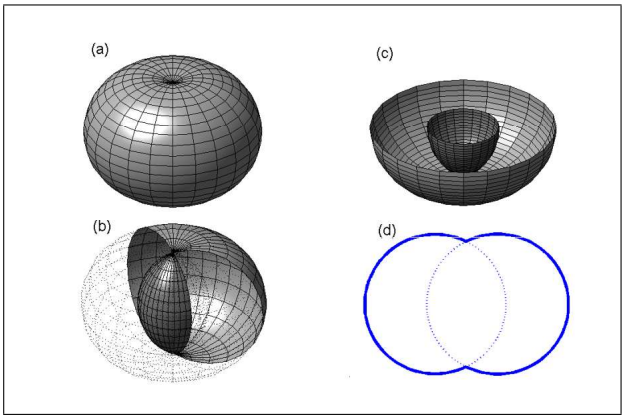



Figure 2. Spindle-torus geometry (a) spindle-torus external surface, (b) a section of external and internal surfaces, (c) a cross-section of the lower part of the surface, (d) an outline of a vertical cross-section of the external surface (solid line) and internal surface (dotted line).

Balmages and Rafaely [4] derived an optimal ratio for the two radii in the dual-sphere configuration, given by

$$\alpha_{opt} = 1 + \frac{\pi}{2kr_{max}}. \tag{12}$$

Due to the similarity between the dual-sphere sampling surfaces and the spindle-torus sampling surfaces, one may consider using the value of $\alpha_{opt}$ in equation (12) for $\alpha_{st}$ in the spindle-torus configuration, thereby avoiding the need for numerical optimization. This is further discussed in section 6.

## 5. Sampling the spindle-torus surfaces

In the previous section the geometry of the spindle-torus surface was characterized. To design a microphone array configuration with high robustness to noise, the sampling scheme of the spindle-torus surfaces has to be defined. Several sampling schemes that offer a trade-off between the required number of samples for implementing an array of order $N$ and the simplicity of their arrangement have been previously presented [8, 12, 13]. Some of these configurations are briefly presented below.

### 5.1. Nearly-uniform sampling

Uniform sampling is a scheme where neighboring samples are distributed with equal distances. The uniform sampling is limited to the five Platonic Solids, which provide up to 20 sampling points. For a nearly-uniform scheme such as the *t-design* [14], the distance between neighboring samples is almost constant. Furthermore, this scheme approximates the integration as summation over the surface of the sphere using equal sampling weights [8]. The advantage of this scheme is the small number of sampling points, i.e. around $1.5\,(N+1)^2$ microphones are required for an array of order $N$. Using unequal sampling weights, other numerically optimized schemes offers designs with an even smaller number of sampling points [15, 13]. Sloan and Womerslay [13] used only $(N+1)^2$ sampling points with the extremal system design for an array of order $N$, which was proven to be the minimal number of sampling points [14].

### 5.2. Gaussian sampling

Gaussian sampling requires $2\,(N+1)^2$ samples, which is higher compared to the nearly-uniform sampling scheme. However, the arrangement of this scheme is much simpler. The azimuth $\phi$ is sampled by $2\,(N+1)$ equally spaced samples that divide the sphere into stripes. The elevation angle $\theta$ requires only $(N+1)$ nearly equally spaced angles [16]. Larger spacing between samples along $\theta$ close to the poles slightly reduces sample density at the poles.

### 5.3. Spindle-torus sampling

The standard schemes described above refer to samples over the surface of a single sphere, whereas in the proposed method samples are placed over the two spindle-torus surfaces. Therefore, in addition to defining the azimuth and elevation of each sample for a given sampling scheme, we also need to determine whether a microphone position is projected to the external or the internal spindle-torus surface. Note that the set of $M$ directions, $(\theta_m, \phi_m)$, $1 \le m \le M$, defined by the sampling scheme are related to the angles of the rotating tables $(\xi_m, \psi_m)$, through equation (9).

The proposed sampling scheme is based on standard Gaussian sampling. Directions of microphone positions are determined by the directions of the Gaussian sampling scheme. The simplicity of the Gaussian sampling scheme allows to define a simple rule for determining which microphone will be placed on which spindle-torus surface. Microphones are alternately projected onto external and internal surfaces, so the four closest neighbors of each sample have different projections from the centered sample. This approach is reasonable as it distributes the samples over the two surfaces in a relatively uniform manner, achieving a large dispersion [11]. This approach was also found to work well in practice. Although some preliminary trials verified the advantage of this approach relative to other approaches, a more complete study of microphone placement on the spindle-torus surfaces is proposed for future work. Because such a study may aim to find configurations that minimize the condition number of matrix $\mathbf{B}$, numerical methods, such as genetic algorithms, may be employed. Comparing the nearly-uniform and the Gaussian sampling schemes, Rafaely [5] has shown that despite having a smaller number of sampling points, the nearly-uniform scheme performs better, i.e., it facilitates a lower condition number. Therefore, sampling methods based on nearly-uniform sampling schemes may be useful. A more comprehensive study of these topics, including ways to distribute samples between the two surfaces, is proposed for future research.



Document downloaded by @DAEL, 2026-11-25 16:42:36 - personal use only

## 6. Simulation study

In this section we present and analyze a specific design example. We will consider a design of an array with 98 sampling points distributed using the alternate Gaussian sampling scheme as described in section 5.C. When designing an array with a spindle-torus configuration, the optimal ratio $\alpha_{st} = \alpha_{opt}$ may be achieved by setting the rotating boom length, $\rho$, and then selecting the mechanical offset, $d$, accordingly. In this example, the length of the rotating boom is set to $\rho = 0.454$ m. The magnitude of $\boldsymbol{J}(\alpha_{st})$ is computed numerically for different mechanical offsets, $d$, which generates different radii ratios. The optimization was done over the range $0 < k\bar{r}_{st} \leq N$, where $\bar{r}_{st}$ denotes the mean radius of the sampling points and $N = 6$ denotes the array order. The optimization result is presented in Figure 3.

The spindle-torus array for this example is designed with mean radii ratio $\bar{r}_{ext}/\bar{r}_{int} = \alpha_{st} = 1.34$, which is around the maximum value of the cost function presented in Figure 3. To achieve this ratio, the length of the mechanical offset was set to $d = 0.095$ m. The mechanical offset, $d$, between the two rotating tables was therefore set to achieve optimal mean radii of the sampling points, cf. equation (10).

A simple alternative to compute $\alpha_{st}$ by numerical optimizations is using the value $\alpha_{opt}$ for the dual sphere array. Applying equation (12) results in $\alpha_{opt} = 1.26$, which is close to the optimal value for the spindle-torus configuration. Figure 3 also shows that the value of the cost function does not decrease significantly for values away from the optimum. This example therefore suggests that the spindle-torus configuration may not be too sensitive to variations in the value of the radii ratio. Although the behavior of matrix **B** in this example and the similarity to the dual-sphere configuration is well explained by the similarity in the geometry of the two configurations, a further study may be required to investigate the specific behavior of spindle-torus arrays with other parameters.

The robustness of the spindle-torus microphone array with the proposed alternate Gaussian sampling scheme is examined next by computing the condition number of matrix **B** for orders in the range $0 \leq n \leq 3$ and over the frequency range of $0 \leq k\bar{r}_{st} \leq N$. The condition number for the spindle-torus microphone array is compared to the condition number of different spherical array configurations with a similar sampling scheme. Figure 4 presents a comparison between the condition number for a spindle-torus configuration with 98 microphones distributed according to the alternate Gaussain sampling scheme; the rigid and the single-sphere configurations with the standard Gaussian scheme for 98 microphones; and the dual-sphere configuration with 98 microphones distributed using the Gaussian sampling scheme on each sphere resulting in a total of 196 microphones. The figure illustrates that the spindle-torus microphone array configuration overcomes the ill-conditioning problem of the single-sphere configuration. Furthermore, the spindle torus achieves high robustness, similar to the dual-sphere array configuration, with half the number of microphones. As previously mentioned in section 5, a more optimal sampling scheme can perform better then the alternate Gaussian scheme. As another comparison, an additional extremal sampling scheme [13] with the spindle-torus configuration is presented in Figure 4. For this sampling scheme an extremal system of 49 microphones is distributed on each of the two spindle-torus surfaces; thus a total of 98 microphones is used for this scheme. As expected, the optimal microphone distribution of the extremal spindle-torus array outperforms the alternate Gaussian spindle-torus configuration.

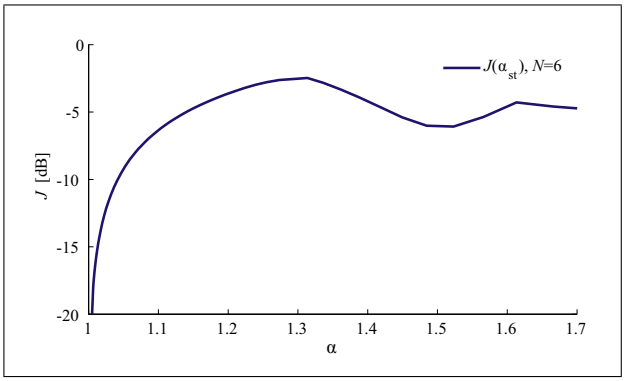



Figure 3. The value of the cost function defined in equation (11) as a function of the radii ratio, $\alpha$.

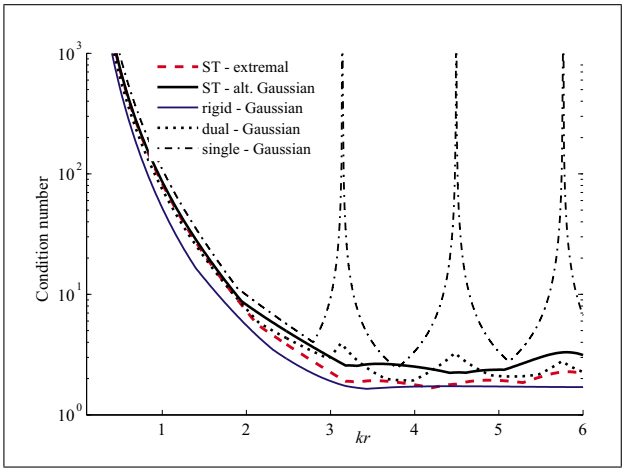



Figure 4. Condition number of matrix **B** of orders $0 \leq n \leq 3$, with samples distributed according to extremal sampling on a spindle torus with 98 samples, and with samples distributed based on a Gaussian sampling scheme, with a spindle torus and 98 samples, a rigid sphere and 98 samples, a single sphere and 98 samples, and a dual sphere and 196 samples, all sampled with an array of order $N = 6$.

## 7. Experiment Example

### 7.1. Experimental procedure

To experimentally validate the proposed spindle-torus scanning microphone array configuration, we present an experiment with a real spindle-torus based scanning microphone array system. Based on the simulation in the pre-



Document downloaded by @DAEL, 2026-11-25 16:42:36 - personal use only

vious section, we consider the design of an array of order $N = 6$, with 98 microphones distributed in accordance with the proposed alternate Gaussian sampling scheme. The length of the rotating boom is set to $\rho = 0.454\,\mathrm{m}$. The mechanical offset, $d$, between the two rotating tables is set to achieve optimal mean radii of the sampling points, as previously described in section 6. The spindle-torus array was designed with a mean radii ratio $\bar{r}_{ext}/\bar{r}_{int} = \alpha_{st} = 1.34$, so the length of the mechanical offset was set to $d = 0.095\,\mathrm{m}$. The mean radius for this configuration is $\bar{r}_{st} = 0.45\,\mathrm{m}$. A second array configuration was then designed, as a reference for comparing the performance of the two arrays. This second configuration was designed by setting the mechanical offset to $d = 0\,\mathrm{m}$, to achieve a single-sphere configuration. In the single-sphere configuration all microphones are at the same radius $r_{single}$. To allow comparison between the two array designs, the length of the rotating boom was now set to $\rho = 0.45\mathrm{m}$, and so $r_{single} = \bar{r}_{st}$. Similar to the spindle-torus array, the single-sphere array was designed as an array of order $N = 6$, with 98 microphones. For the single-sphere array the microphones were distributed using the standard Gaussian sampling scheme.

The spindle-torus array and the single-sphere array were placed in an anechoic chamber with internal dimensions 2x2x2 m. The chamber was made by Eckel Industries Inc. and was certified as anechoic above 300Hz. It is located at the Acoustics Laboratory at Ben Gurion University. The tested microphone arrays were realized based on a single scanning Bruel&Kjaer pressure microphone, type 4942, with positioning accuracy of $\pm 0.5^o$. A Genelec 8030A speaker was used as a sound source. The sound field measured by the microphone was recorded using an M-audio *fast track pro* 2-channels audio interface, connected to a personal computer. The microphone array was centered at $(x_0, y_0, z_0) = (0, 0, 0)$, which corresponds to the center of the anechoic chamber. Positioning of the array and the loudspeaker as well as the orientation of the array was performed using a measuring tape. Although the accuracy of this positioning method is limited, for this experiment the effect of an error in the orientation will be a circular shift of the result. However, the microphone array system performance is strongly affected by the spatial placement of microphone sensors. It is thus linked to the precision of the scanning microphone's mechanical positioning system. The sound source was placed at $(x_{src.}, y_{src.}, z_{src.}) = (-0.58, 0.6, 0.45)\mathrm{m}$, that is in the direction $(\theta_l, \phi_l) = (66^o, 134^o)$. Due to the small dimensions of the anechoic chamber the loudspeaker was close to the scanning microphone array. The acoustic center of a loudspeaker is driver and frequency-dependent and does not correspond to the geometric center. It thus might result in frequency-dependent errors in source direction estimations. In the applied configuration these errors are limited to about 2 degrees. The source played a chirp-sine signal. microphone was placed in space using the two rotating tables, according to the array sampling scheme.

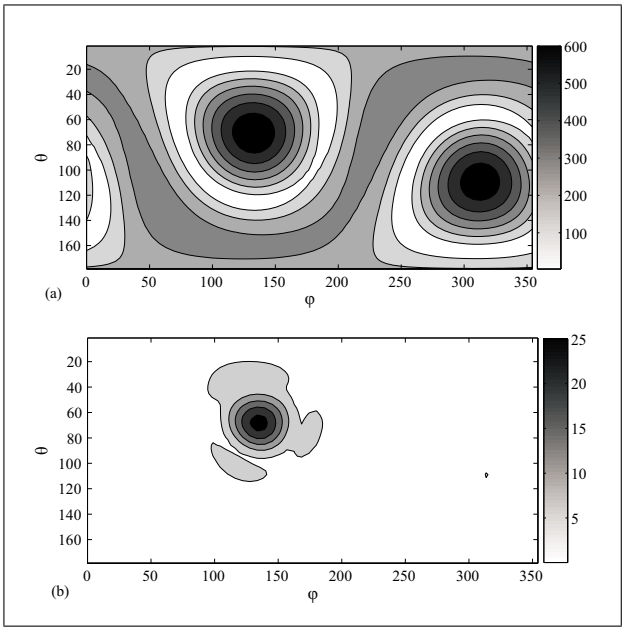



Figure 5. Spatial amplitude density at 699Hz, for (a) single-sphere array, and (b) spindle-torus array.

The microphone signal, along with the loudspeaker input signal, were recorded by the computer and the data was later used to compute the frequency response between the loudspeaker input and the output of the microphone at each position. This experimental procedure is based on an experiment that was previously presented by Rafaely et al.[17].

### 7.2. Experiment results

Plane wave decomposition was calculated as in section 2; the result is the spatial amplitude density $a(k, \theta, \phi)$. In Figures 5 and 6 we present $a(k, \theta, \phi)$ at different frequencies to compare the performance of spindle-torus and single-sphere scanning microphone array configurations. The array performance is analyzed at $f_1 = 699\,\mathrm{Hz}$ and $f_2 = 630\,\mathrm{Hz}$. The values of $kr$ for these frequencies are $k_1 r = 5.77$ and $k_2 r = 5.2$, respectively. Due to the anechoic conditions only a sound wave coming from a single direction should appear in the analysis. The spatial amplitude density $a(k, \theta, \phi)$ is therefore expected to include only one significant peak at the direction of the sound source $(\theta_l, \phi_l) = (66^o, 134^o)$.

The single-sphere configuration at 699Hz is considered first. Figure 5a shows two peaks and a wide-stretched maximum between them, which do not correspond to the direction of the source. Therefore, this figure does not present the expected spatial amplitude density at this frequency. The value of $kr$ for this array is $k_1 r = 5.77$. Figure 4 suggests that the open-sphere configuration suffers from ill-conditioning at $k_1 r = 5.77$, which means poor robustness to noise. This ill-conditioning is due to a zero of the spherical Bessel function $b_2(k_1 r)$. The spatial amplitude density $a(k, \theta, \phi)$ in Figure 5a therefore represents a second order spherical harmonic pattern $Y_2^0$. The spindle-torus configu-



Document downloaded by @DAEL, 2026-11-25 16:42:36 - personal use only

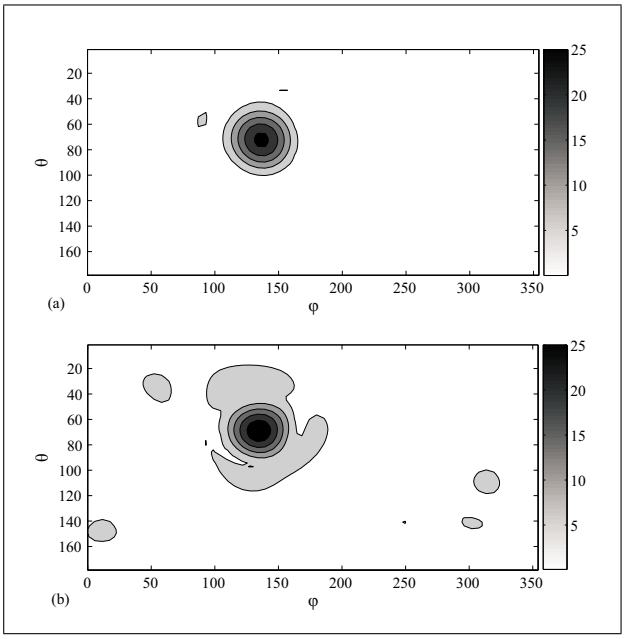



Figure 6. Spatial amplitude density at 630Hz, for (a) single-sphere array, and (b) spindle-torus array.

ration at the same frequency is considered next. The spatial amplitude density is presented in Figure 5b showing one clear peak very close to the direction of the source, as expected. The spindle-torus configuration therefore overcame the ill-conditioning of the single sphere at zero frequency.

At the second analyzed frequency $f_2 = 630\,\text{Hz}$, the plane wave decomposition result in Figure 6b, for the spindle-torus configuration, is very similar to the one in Figure 5b. This illustrates the robustness of the spindle-torus array to noise at different frequencies. However, in this case the plane wave decomposition result of the single-sphere is also good. Even though the spatial amplitude density for the two configurations shows a clear peak at the exact direction of the source, comparing Figures. 6a and 6b one may notice that at this frequency, the single-sphere configuration presents a peak with slightly less noise around it.

## 8. Conclusion

This paper presented a new spherical array configuration. This configuration is based on the shape of a spindle torus and achieves high array robustness to noise with a relatively small number of sampling points. It also proposes an implementation of the mechanical system, where no adjustment of boom length is required within a measurement session. Methods for the design and implementation of such an array for different orders or sizes are given, making the array usable in practice for various applications. An experimental example is presented to demonstrate the performance and the advantages of the spindle-torus array.

### Acknowledgment

This research is partly supported by the Israel Science Foundation (ISF grant no. 155/06).

### References

[1] J. Meyer, G. W. Elko: A highly scalable spherical microphone array based on an orthonormal decomposition of the sound field. Proceedings ICASSP **II** (2002) 1781–1784.

[2] T. D. Abhayapala, D. B. Ward: Theory and design of high order sound field microphones using spherical microphone array. Proceedings ICASSP **II** (2002) 1949–1952.

[3] B. Rafaely: Plane-wave decomposition of the pressure on a sphere by spherical convolution. J. Acoust. Soc. Am. **116** (2004) 2149–2157.

[4] I. Balmages, B. Rafaely: Open-sphere designs for spherical microphone arrays. IEEE Trans. Audio, Speech and Lang. Proc. **15** (February 2007) 727–732.

[5] B. Rafaely: The spherical-shell microphone array. IEEE Trans. Audio, Speech and Lang. Proc. **16** (May 2008) 740–747.

[6] A. Gray, E. Abbena, S. Salamon: Modern differential geometry of curves and surfaces with mathematica, 3rd ed. CRC Press, 2006.

[7] D. Alon, B. Rafaely: Efficient sampling for scanning spherical array. Paris, France, May 2010, Proc. of the 2nd International Symposium on Ambisonics and Spherical Acoustics.

[8] B. Rafaely: Analysis and design of spherical microphone arrays. IEEE Trans. Speech Audio Proc. **13** (January 2005) 135–143.

[9] E. G. Williams: Fourier acoustics: Sound radiation and nearfield acoustic holography. Academic Press, London, UK, 1999.

[10] G. Arfken: Mathematical methods for physicists. Academic Press, New York, 1985.

[11] S. M. LaValle: Planning algorithms. Cambridge University Press, 2006.

[12] Z. Li, R. Duraiswami: Flexible and optimal design of spherical microphone arrays for beamforming. IEEE Trans. Audio, Speech and Lang. Proc. **15** (2007) 702–714.

[13] I. H. Sloan., R. S. Womersley: Extremal systems of points and numerical integration on the sphere. Adv. Comp. Math. **21** (July 2004) 107–125.

[14] R. H. Hardin, N. J. A. Sloane: Mclaren's improved snub cube and other new spherical designs in three dimensions. Discrete Computational Geometry **15** (April 1996) 429–441.

[15] J. Fliege, U. Maier: The distribution of points on the sphere and corresponding cubature formulae. IMA J. Numer. Anal. **19** (1999) 317–334.

[16] M. J. Mohlenkamp: A fast transform for spherical harmonics. The Journal of Fourier Analysis and Applications **5** (1999) 159–184.

[17] B. Rafaely, I. Balmages, L. Eger: High-resolution plane-wave decomposition in an auditorium using a dual-radius scanning spherical microphone array. J. Acoust. Soc. Am. **12** (November 2007) 2661–2668.



*Document downloaded by @DAEL, 2026-11-25 16:42:36 - personal use only*